

**Multicolour electrochromic film based on a TiO₂@ poly[Ni(*salen*)]
nanocomposite with excellent electrochemical stability**

Marta Nunes^{a*}, Cosme Moura^b, A. Robert Hillman^c and Cristina Freire^{a*}

^a REQUIMTE/LAQV, Departamento de Química e Bioquímica, Faculdade de Ciências, Universidade do Porto, 4169-007 Porto, Portugal.

^b CIQ, Departamento de Química e Bioquímica, Faculdade de Ciências, Universidade do Porto, 4169-007 Porto, Portugal (cnmoura@fc.up.pt).

^c Department of Chemistry, University of Leicester, Leicester LE1 7 RH, UK (arh7@leicester.ac.uk).

*Corresponding author: Professor Cristina Freire (acfreire@fc.up.pt), Dr. Marta Nunes (marta.nunes@fc.up.pt)

Tel.: +351 22 04020590; Fax: +351 22 0402 695

ABSTRACT

We report the electrochromic properties of a polymeric nanocomposite prepared by potentiodynamic deposition of the transition metal complex [Ni(3-Mesalen)], designated as [1], in the presence of TiO₂ nanoparticles (NPs) with average size of 9.7 ± 1.1 nm.

Entrapment of TiO₂ NPs in the poly[1] matrix was confirmed by several techniques. The nanocomposite TiO₂@poly[1] films showed similar electrochemical responses to the original (nanoparticle-free) poly[1] films, but with higher electroactive surface coverages (Γ), showing the advantage of the nanocomposite preparation. The results indicated that the electronic structure of poly[1] was retained in the nanocomposite; nonetheless, a lower ε -value was obtained for the charge-transfer band of the former, revealing superior stability of the nanocomposite for ligand high oxidation states.

The TiO₂@poly[1] nanocomposite showed interesting colour changes, from yellow (reduced state) to green and russet (oxidised states), with enhanced electrochemical stability, demonstrated by a charge loss of only 7.3 % over ca. 10,000 redox cycles surpassing the original polymer film stability: the loss of electroactivity is a factor of ca. two less than for pristine poly[1]. Furthermore, an enhancement of 16.7 % in the optical modulation ($\Delta OD = 0.48$) was also observed for the nanocomposite, confirming the benefit of TiO₂ incorporation into the EC properties of the original polymer film.

Keywords: Electrochromism; Electroactive polymers; TiO₂ nanoparticles; Hybrid films; Polymeric nanocomposites.

INTRODUCTION

In recent years, the continuous development of new technologies has demanded materials and structures with specially tailored properties.¹ In this context, nanohybridization of a conducting organic polymer and a metal oxide semiconductor has been recognized as one of the most attractive combinations of organic/inorganic composite structures.² The new nanohybrids have the advantages of combining individual semiconducting functions from the polymer and the metal oxide (p/n junction),³ and of combining the elasticity and functionality of the former with the high thermal and chemical stability of the latter, leading to new composite materials with synergistic or complementary behaviors.^{4,5} The interesting properties of these nanohybrids make them viable candidates for diverse applications, including solar cells,⁶ electrochemical capacitors,^{7,8} lithium batteries,⁹ water splitting,¹⁰ sensors¹¹ and electrochromic devices.¹²

Electrochromism is broadly defined as a reversible change in the optical properties of a material induced by an external voltage.¹³ Short switching times, large optical modulation and long-term cyclic stability are the most important requisites for the application of electrochromic devices (ECDs) in light and overheating protection windows, mirrors and display panels.^{14,15} Conducting polymers (CPs) are a widely studied class of electrochromic (EC) materials¹⁶ that, in addition to good mechanical properties and potential low cost, show interesting optical properties due to their multiple redox states, with rich color changes and ease of color tuning via structural modification of the monomers.¹⁷⁻¹⁹ Unfortunately, the rate of interconversion between redox states is limited by the slow transport of counter ions into the EC layer to satisfy electroneutrality.²⁰ This drawback can be overcome by the combination of CPs with organized metal oxide nanostructures, in order to take advantage of the high surface-to-volume ratio and short diffusion distances for ion/electron transport of the latter, which

promotes fast reaction kinetics and fast switching speed.^{5, 20} Further, metal oxides generally exhibit the advantages of good electrochemical stability and excellent switching reversibility.⁵ Therefore, a synergistic combination of the merits of CPs and metal oxides promises an opportunity to develop new hybrid materials with improved EC properties, in which CP redox chemistry provides the coloration change and the metal oxide enhances the electronic transport through the metal oxide conduction band.^{2,21}

Among metal oxides, titanium dioxide (TiO₂) is one of the most investigated wide gap semiconductors, due to its low cost, non-toxicity and good chemical stability.^{22,23} The ability of TiO₂ to act as an electron acceptor - to form electron donor-acceptor pairs by interaction with a p-type CP - raises the possibility that the changes induced by its incorporation go well beyond mere compositional and morphological modifications.²⁴ In recent years, some examples of TiO₂/CPs hybrids have been reported as new EC materials through the combination of TiO₂ with polyaniline (PANI),^{20,24,25} polypyrrole² and poly(3,4-ethylenedioxythiophene):poly(styrene sulfonic acid) (PEDOT:PSS).¹³ In general, the nanocomposites obtained showed faster response times and higher optical contrasts, colouration efficiencies and electrochemical stability.

In this work we extend this concept to the M(*salen*)-based (M ≡ transition metal) family of CPs. Specifically, we report the preparation and characterization of hybrid films based on the incorporation of TiO₂ NPs into the matrix of poly[Ni(3-Mesalen)] films ([Ni(3-Mesalen)] is *N,N'*-bis(3-methylsalicylideneimine) nickel(II)) and the evaluation of their EC properties. Poly[Ni(3-Mesalen)], hereafter designated poly[1], belongs to the class of electroactive metallopolymers poly[M(*salen*)] that, despite the presence of a transition metal, show significant resemblances to the polyaromatic CPs indicated above. Recently, their EC properties have been studied and explored to EC device fabrication.^{26,27} In particular, the EC performance of pristine poly[Ni(3-Mesalen)]²⁸

showed promising results, with an acceptable electrochemical stability (retaining over 65% charge recovery after ≈ 9000 cycles) and interesting colour changes (from yellow in neutral state to green and russet (reddish-brown) in oxidised states). However, to realize practical commercial application, the EC properties of poly[1] need to be further improved. Analogous to conventional CPs, this can be pursued by preparation of composites with semiconductors. Thus, in this paper, we explore the effect on EC properties of the incorporation of TiO₂ NPs into the host polymeric film. TiO₂ is an n-type semiconductor, with a band gap of ≈ 3.2 eV,²⁹ similar to that of the pristine polymer film (≈ 3.8 eV). The influence of TiO₂ NPs loading on the electrochemical response and the structural, morphological and optical properties of the TiO₂@poly[1] nanocomposite film was evaluated.

EXPERIMENTAL SECTION

Materials and instrumentation

Titanium (IV) isopropoxide (TTIP, Aldrich, ≥ 97.0 %), LiClO₄ (Aldrich, 99 %), isopropanol (VWR, 99.7 %), ethanol absolute (Fisher Chemical, 99.99 %), nitric acid (Panreac, 65 %), and acetonitrile and propylene carbonate (PC) (Romil, pro analysis grade) were used directly as received; ultra-pure water (resistivity 18.2 M Ω cm at 25 °C, Millipore) was used. The complex *N,N'*-bis(3-methylsalicylideneimine) nickel(II), [Ni(3-Mesalen)], and the respective *salen* ligand were prepared by methods described in the literature.³⁰ Briefly, the *salen* ligand H₂(3-Mesalen) was synthesized by refluxing a methanolic solution containing ethylenediamine and 2-hydroxy-3-methylbenzaldehyde (molar ratio = 2:1); on cooling to room temperature, the yellow solid formed was filtered off and dried under vacuum. The complex [Ni(3-Mesalen)] was prepared by refluxing a

methanolic solution containing stoichiometric amounts of nickel (II) acetate and the ligand H₂(3-Mesalen); after cooling, a red-brown solid was obtained.

Powder X-ray diffraction (XRD) measurements of TiO₂ NPs were performed at Departamento de Química, CQ-VR, Universidade de Trás-os-Montes e Alto Douro (Vila Real, Portugal), at room temperature using a PW 3040/60 X'Pert Pro Röntgen diffractometer with Cu K α radiation ($\lambda = 1.5418 \text{ \AA}$) and $\theta/2\theta$ Bragg-Brentano configuration, over the 2θ range of 15–80°. The system includes the ultrafast PW3015/20 X'Celerator detector and a secondary monochromator. The diffractograms were treated with Rietveld refinement. The XRD analysis of film samples were performed at Departamento de Física e Astronomia, Faculdade de Ciências da Universidade do Porto, Porto, Portugal, at room temperature using a Smartlab diffractometer (Rigaku, D-tex ultra 250 detector) with Cu K α radiation ($\lambda = 1.5406 \text{ \AA}$) and $\theta/2\theta$ Bragg-Brentano configuration.

X-ray photoelectron spectroscopy (XPS) analyses were performed at CEMUP (Porto, Portugal), in a Kratos AXIS Ultra HSA spectrometer, using a monochromatic Al K α radiation (1486.7 eV). The raw XPS spectra were deconvoluted with the XPSPEAK 4.1 software, using a non-linear least squares fitting routine after a Shirley-type background subtraction. To correct possible deviations caused by electric charge of the samples, the C1s peak at 284.6 eV was taken as internal reference. The surface atomic percentages were calculated from the corresponding peak areas, using sensitivity factors provided by the manufacturer.

Fourier transform infrared (FTIR) spectra were obtained on a Jasco FT/IR Plus Spectrophotometer in the 2000 – 400 cm⁻¹ region, with a resolution of 4 cm⁻¹ and 32 scans. The samples were diluted with KBr (99 %, spectroscopic grade, Sigma-Aldrich) and studied as pellets containing 1.2 wt. % of sample.

The UV-Vis spectra were recorded on a Shimadzu UV-3600 spectrophotometer in the 250 -700 nm range, using quartz cells with a path length of 10 mm.

Transmission electron microscopy (TEM) images were collected at Departamento de Química, CQ-VR, Universidade de Trás-os-Montes e Alto Douro (Vila Real, Portugal), with a LEO 906E microscope at 120 kV. The sample was prepared by using a TiO₂ NPs ultra-pure water dispersion in a carbon-coated 400 mesh copper grid. The diameter of 100 particles was measured to generate a histogram to calculate the average particle size.

The Scanning Electron Microscopy / Energy-Dispersive X-Ray Spectroscopy (SEM/EDS) analyses were performed at CEMUP, using a high-resolution scanning electron microscope with X-Ray microanalysis and electron backscattered diffraction analysis (JEOL JSM 6301F/ Oxford INCA Energy 350).

Electrochemical studies were performed using an Autolab PGSTAT 30 potentiostat/galvanostat (EcoChimie B.V.), controlled by GPES software. The studies were performed using a three-electrode cell, with single or separate (chronoamperometric studies) compartments, using an Ag/AgCl (NaCl / 1.0 mol dm⁻³) electrode (Metrohm ref. 6.0724.140) as the reference electrode, a Pt wire or a Pt plate (for separate compartment cell) as the counter electrode and poly(ethyleneterephthalate) (PET) coated with indium tin oxide (ITO) (ITO/PET) (Aldrich, resistivity of 60 Ω sq⁻¹) as the working electrode. In the coulometric studies the working electrode was a Pt disk (area 0.0314 cm², BAS).

The spectroelectrochemical studies were performed *in situ* using an Agilent 8453 spectrophotometer (with diode array detection) coupled to the potentiostat/galvanostat. As experimental apparatus was used a teflon cell with an Ag/AgCl (NaCl / 3.0 mol dm⁻³) (Bio-Logic) reference electrode, a Pt grid counter electrode and ITO/PET (typical area 0.785 cm²) as working electrode.

The CIELAB coordinates were acquired on a reflectance spectrophotometer Konica Minolta Sensing CM-2600d, in the range 350-750 nm during five sequential measurements, considering an area of 8 mm diameter. The calibration of the spectrophotometer was performed with white and black reference standards.

Synthesis and characterization of TiO₂ NPs

The synthesis of TiO₂ NPs was performed by a procedure adapted from the literature.³¹ A solution of TTIP (5 mL) in isopropanol (15 mL) was added drop by drop to a solution of millipore water (250 mL) at pH 2 (adjusted with HNO₃), under vigorous magnetic stirring. The turbid solution formed immediately was heated up to 65 °C for 6 h. The product was washed with ethanol and dried for 1 day. Finally, the powder was annealed at 300, 400 and 500 °C for 2 h (60 °C / hour). According to the annealing temperature, the samples are designated TiO₂_300, TiO₂_400 and TiO₂_500, respectively.

The TiO₂ NPs were fully characterized by XRD, TEM, XPS, FTIR and UV-Vis and the results are detailed described in Supporting Information, SI.

The band gap, E_g , of TiO₂ NPs was determined through the Equation (1):

$$\alpha = A (hv - E_g)^n / hv \quad (1)$$

where α is the absorption coefficient, A is a constant, hv is the energy of light and $n=2$, assuming an indirect transition). The band gap was extrapolated from the $(\alpha hv)^{1/2}$ vs. hv plot, considering a proportional relation between α and the Kubelka-Munk function $F(R)$.³²⁻³⁴

Nanocomposite film preparation and electrochemical characterization

The TiO₂@poly[1] nanocomposite films were prepared by CV from deposition solutions containing 1.0 mmol dm⁻³ [Ni(3-Mesalen)] and 5, 15 or 25 wt.% (TiO₂/LiClO₄ wt.%) of TiO₂_400 NPs in 0.1 mol dm⁻³ LiClO₄/CH₃CN. Prior to electrodeposition, the starting solutions were (i) sonicated for 10 minutes or (ii) sonicated for 10 minutes followed by reflux for 3 hours. To accomplish electrodeposition, the potential of the working electrode (ITO/PET 2.25 cm²) was cycled between 0.0 and 1.3 V (at $\nu = 0.020$ V s⁻¹) or -0.2 and 1.3 V (at $\nu = 0.100$ V s⁻¹) for 10 scans. According to the method used, the resultant films were designated TiO₂@poly[1]_s and TiO₂@poly[1]_r (s = sonicated and r = refluxed), respectively. The pristine poly[1] film was prepared using the same experimental conditions, but in the absence of TiO₂ NPs.

After film deposition, the modified electrodes were rinsed with dry CH₃CN, immersed in a monomer- and TiO₂-free 0.1 mol dm⁻³ LiClO₄/CH₃CN solution and were firstly conditioned by recording the cyclic voltammograms until a constant voltammetric response is obtained (typically 5 cycles), in the potential range -0.1 to 1.3 V, $\nu = 0.020$ V s⁻¹. The electroactive surface coverage, Γ / nmol cm⁻² (cited in terms of monomeric units) of each film was determined by a coulometric assay,^{35,36} using cyclic voltammograms (CVs) obtained in 0.1 mol dm⁻³ LiClO₄/CH₃CN solution. Strictly, this is the electronically accessed population on the experimental timescale; for this aspect, a slow scan rate of $\nu = 0.01$ V s⁻¹ was used, to ensure complete film redox conversion. The doping level (n) values used for Γ determination were calculated from comparison of coulometric data for films deposition and cycling, as described in the literature,^{35,36} and were found to be $n = 0.65$ and 0.48 for films prepared at $\nu = 0.020$ and 0.100 V s⁻¹, respectively.

The pristine and nanocomposite films prepared with a TiO₂ loading of 5 wt.% at $\nu = 0.020$ V s⁻¹, were also voltammetrically characterized in 0.1 mol dm⁻³ LiClO₄/PC, at $\nu = 0.010$ V s⁻¹ for 3 redox cycles, in the same potential range. Note that all the mentioned

TiO₂ loadings - “wt.% TiO₂” - refer to the deposition feedstock, *i.e.* the loading in the deposition solution; it is used for nomenclature purposes only, not as a claim that this is the film content, as it was not possible to have accurate information on the fraction present in the resulting film.

Composition and textural characterization

The composition and textural characterizations of TiO₂@poly[1]_r nanocomposites were performed by XPS, SEM/EDS and XRD (TiO₂@poly[1]_s was not characterised since presented lower TiO₂ loading). The films were prepared with 5 wt.% of TiO₂_400 NPs at $\nu = 0.020 \text{ V s}^{-1}$, and analysed after emersion in the reduced state (application of $E = 0.0 \text{ V}$ for 200 s). Specifically for the films analysed by XRD, a Pt plate (area = 2.0 cm²) was used as the working electrode.

Films subjected to potential cycling in 0.1 mol dm⁻³ LiClO₄/CH₃CN and 0.1 mol dm⁻³ LiClO₄/PC (voltage regime as above), were also analysed by XPS in order to investigate the influence of successive redox switching in the chemical composition. Pristine poly[1] films were prepared in identical conditions and studied for comparison.

The nanocomposite film was analysed by SEM/EDS in two different perspectives: (i) in cross-section (“vertical” section) and (ii) in plane view (“horizontal section”) of the internal structure of the polymeric film. For (i) the film was subjected to a cut perpendicular to the surface, while in (ii) a part of the film surface was removed (using a carbon conductive tape), exposing the inside of the polymeric film.

Spectroelectrochemical characterization

In situ UV-Vis spectroscopy was performed with films prepared with 3 electrodeposition cycles, at $\nu = 0.020 \text{ V s}^{-1}$, from a deposition solution containing 5 wt.%

of TiO₂ NPs (except for pristine film). The films were cycled between -0.1 and 1.3 V, $\nu = 0.020 \text{ V s}^{-1}$, using LiClO₄/PC 0.1 mol dm⁻³ as supporting electrolyte. The UV-Vis spectra were acquired simultaneously, at intervals of 0.5 s (i.e. at 10 mV potential resolution), in the wavelength range 315 to 1100 nm, during the 4th redox cycle. The molar extinction coefficients, $\varepsilon / \text{cm}^{-1} \text{ mol}^{-1} \text{ dm}^3$, of all electronic bands were estimated using a combination of the Beer-Lambert and Faraday laws (Equation 2):³⁵⁻³⁷

$$Abs(\lambda) = \varepsilon(\lambda) Q / nFA \quad (2)$$

where Q is the charge (C), n is the doping level, F is the Faraday constant and A the area (cm²).

Electrochromic property evaluation

EC properties were evaluated for TiO₂@poly[1]_r films, prepared with 5 wt.% of TiO₂ NPs, at $\nu = 0.020 \text{ V s}^{-1}$, by 10 or 3 (chronoabsorptometric study) electrodeposition cycles. The studies were performed in LiClO₄/PC 0.1 mol dm⁻³ supporting electrolyte, considering the colour change yellow ↔ green (that proved to be the most promising for the pristine poly[1]).²⁸ The electrochemical stability tests were performed by chronoamperometry, applying two potential steps of 50 s by redox cycle, with potential alternating between 0.0 and 0.7 V, for a long period of time (9500 redox cycles, ≈ 11 days). The switching times were determined from the chronocoulograms (obtained through the chronoamperograms), based on 90% of the full charge change, as the correspondence between switching times determined from charge and optical change was already reported for pristine poly[1].²⁸ The remaining EC parameters were determined through the chronoabsorptograms obtained during the monitoring of the chronoamperometric experiment by UV-Vis spectroscopy; the measurements were performed at the fixed wavelength of $\lambda = 750 \text{ nm}$, acquiring the UV-Vis spectra with

intervals of 1 s. The change of the optical density, ΔOD , was estimated using the Equation 3:³⁸

$$\Delta OD(\lambda) = \log(T_{\text{red}}(\lambda) / T_{\text{ox}}(\lambda)) \quad (3)$$

where T_{red} and T_{ox} are the transmittance values of the films in reduced and oxidised states, respectively, at $\lambda = 750$ nm. The colouration efficiency ($\eta / \text{cm}^2 \text{C}^{-1}$) was measured by the relation between ΔOD and the amount of injected/ejected charge per unit area, Q_d , necessary to induce the full switch, given by the Equation 4:^{38,39}

$$\eta = \Delta OD / Q_d \quad (4)$$

The CIELAB values were determined after exposing the polymeric films to the application of a constant potential value ($E = 0.0, 0.7$ or 1.3 V) during 50 s, in LiClO_4/PC . The CIELAB coordinates are based on colour matching (CIE system) by a linear combination of three “virtual” primary colours X, Y and Z. Because the values of this colours are not visually uniform, a non-linear transform follows, resulting in opponent-type coordinates L^* , a^* and b^* . The parameter L^* represents lightness (in a scale ranging from 0 (black) to 100 (white)), a^* red-greenness and b^* yellow-blueness.²⁶ The total colour difference (ΔE^*) between two different oxidation states of a film was calculated from L^* , a^* and b^* values, using the Equation 5:⁴⁰

$$\Delta E^* = ((\Delta L^*)^2 + (\Delta a^*)^2 + (\Delta b^*)^2)^{1/2} \quad (5)$$

where $\Delta x^* = x^*_{\text{more oxidized state}} - x^*_{\text{less oxidized state}}$ ($x^* = L^*, a^*$ or b^*).

RESULTS AND DISCUSSION

Electrochemical preparation and characterization of $\text{TiO}_2@\text{poly}[1]$

The $\text{TiO}_2@\text{poly}[1]$ films were potentiodynamically polymerized from deposition solutions containing the monomer $[\text{Ni}(3\text{-Mesalen})]$ and TiO_2_{400} NPs (NPs with average

particle size of 9.7 nm (± 1.1 nm), see SI) at different loadings (5, 15 and 25 wt.%), using two scan rates ($\nu = 0.020$ or 0.100 V s^{-1}) (Figure 1 (a)). With the different electropolymerization conditions we endeavour to optimize not only the quantity of entrapped TiO_2 , but also its homogeneity within the polymer supramolecular structure.

Figure 1 (b) shows representative voltammetric responses during nanocomposite electropolymerization; we choose to sample the 10th electropolymerization cycles (at $\nu = 0.020 \text{ V s}^{-1}$) for nanocomposite films deposited using 5 wt.% TiO_2 . The analogous results for poly[1] are shown for comparison. To give a pictorial insight into the much larger data matrix acquired, Figure S6 depicts the voltammograms obtained during the entire electropolymerization process for $\text{TiO}_2@\text{poly}[1]_r$ at $\nu = 0.020$ and 0.100 V s^{-1} , with 5 wt.% of TiO_2 NPs. Numerical values for the peak potentials for all films are summarized in Table S1.

The voltammetric responses of nanocomposites prepared at $\nu = 0.020 \text{ V s}^{-1}$ are similar to those of the pristine film, and are comparable for films prepared with different loadings of TiO_2 NPs (Figure 1 (c)), despite small shifts in anodic and cathodic peaks. Analogous behaviour was observed for films electropolymerized at $\nu = 0.100 \text{ V s}^{-1}$ (Figure S7, SI), although the films prepared at this scan rate present the anodic voltammetric peaks shift to less negative potential values and the cathodic peaks shift to more negative potentials, in comparison to films prepared at $\nu = 0.020 \text{ V s}^{-1}$; this effect is more pronounced for the nanocomposites.

Figure 1

The results indicate that poly[1] oxidative electropolymerization mechanism was not changed by the presence of TiO_2 . Thus, the two peaks observed at $E_{\text{pa}} = 0.87\text{-}1.03 \text{ V}$

and $E_{pa} = 1.06-1.18$ V, in the first anodic half-cycle, are attributed to the [Ni(3-Mesalen)] oxidation and subsequent formation of oligomers/polymer in the working electrode surface, while the peaks at $E_{pc} = 0.66-0.70$ V and $E_{pc} = 0.18-0.22$ V, observed in the reverse scan, correspond to the reduction of the as-formed nanocomposite films. The new anodic peak at $E_{pa} = 0.43-0.53$ V, in the second and subsequent scans, is assigned to the oxidation surface-confined polymer film deposited in the previous cycle(s).^{35,36}

The voltammetric responses of nanocomposites (from 5 and 15 wt.% TiO₂-loading media) showed higher current intensities than those of poly[1]. This is attributed to a larger electroactive surface area due to the incorporation of the TiO₂ NPs on the poly[1] structure; however, when the TiO₂ loading media increase to 25 wt.%, the electrochemical responses exhibit lower current intensities, suggesting that there is an optimum TiO₂ loading to maximize electropolymerization efficiency.

The voltammetric responses of TiO₂@poly[1] nanocomposites (prepared at $\nu = 0.020$ V s⁻¹) in LiClO₄/CH₃CN, along with the pristine film, are depicted in Figure 2 (a). The equivalent responses for films prepared at $\nu = 0.100$ V s⁻¹ are shown in Figure S9 (a) and the CVs obtained during the entire film conditioning of TiO₂@poly[1]_r films (with 5 wt.% of TiO₂ loading) are depicted in Figure S8, as representative examples; Table S2 summarizes the peak potential values.

The voltammetric responses of the nanocomposites are similar to those of poly[1], apart from small shifts of peak potentials. The nanocomposite films prepared with different TiO₂-loadings (Figures 2 (b) and S9 (b)) also show similar voltammetric profiles, with the exception of the film electrodeposited at $\nu = 0.020$ V s⁻¹ with 25 wt.% TiO₂ loading, whose CV shows the anodic peak strongly shifted to more positive potentials and the cathodic peaks to more negative potentials, revealing a greater resistance of the nanocomposite film.

Figure 2

Figure 3 shows the electroactive surface coverage, Γ / nmol cm⁻², of films prepared with different TiO₂ loadings and at the two scan rates. The data revealed that the films prepared at $\nu = 0.020$ V s⁻¹ have higher Γ than those prepared at $\nu = 0.100$ V s⁻¹. This is qualitatively consistent with the fact that the slower scan rate experiment involves longer periods of time in the polymerization range. Moreover, nanocomposite films present higher Γ than the respective pristine film, deposited at the same scan rate, which is in agreement with the higher current intensities observed in nanocomposites cycling voltammograms and indicates the successful incorporation of the TiO₂ on poly[1] matrix; in the most of cases, Γ -values are higher for TiO₂@poly[1]_r nanocomposites. For films prepared at $\nu = 0.020$ V s⁻¹, Γ increases significantly from poly[1] to nanocomposites deposited with 5 and 15 wt.% TiO₂ loading, decreasing after for films with 25 wt.%. These results suggest an optimal TiO₂ loading, from which higher loadings may be unfavourable and prevent the deposition of Ni-*salen* polymer; this behaviour has been also observed for WO₃ films loaded with carbon nanotubes.⁴¹ For films prepared at $\nu = 0.100$ V s⁻¹, the increase of Γ -values from pristine film to nanocomposites and between the nanocomposites (prepared with different TiO₂ loadings) was lower than the observed for films prepared at $\nu = 0.020$ V s⁻¹, which can indicate a lower incorporation of TiO₂ NPs at this scan rate. This observation is supported by the fact that the metal oxide incorporation into the films is limited by their mass transport and, so, favoured by slower polymerization procedures.²¹

Figure 3

Taking into account the Γ values obtained and the voltammetric profiles (similar current intensities for both nanocomposite films with 5 and 15 wt.%, but shift of the anodic/cathodic peaks for less and more negative potential values, respectively, with the loading increase, Figure 2(b)), films prepared at $\nu = 0.020 \text{ mV s}^{-1}$ with 5 wt.% of TiO_2 loading ($\Gamma = 240 / 270 \text{ nmol cm}^{-2}$) were employed to pursue further studies.

In Figure 4, the CVs obtained during the cycling (3rd scan) of the poly[1] and TiO_2 @poly[1] films in LiClO_4/PC are shown, as this supporting electrolyte promotes the highest electrochemical stability for poly[1] film;²⁸ in Table S3 the peak potential values are summarised. The nanocomposites show similar electrochemical responses to that of pristine film but higher current intensities, similarly to that observed in $\text{LiClO}_4/\text{CH}_3\text{CN}$, although the peaks are less defined in LiClO_4/PC .

During redox cycling, the nanocomposites showed the typical electrochromic behaviour of poly[1], exhibiting colour changes between yellow, green and russet according with the applied potential, as depicted in the insets of Figure 4.

Figure 4

Composition and textural properties

In Figure 5, SEM micrographs of (a) a cross-section (“vertical” cut) and (b) interior plan (“horizontal” cut, plane view) are depicted for the study of the TiO_2 @poly[1]_r nanocomposite internal structure.

Figure 5

Both micrographs show the continuous layer with irregular surfaces, characteristic of the pristine poly[1].²⁸ Through the cross-section micrograph (Figure 5 (a)), the thickness of the nanocomposite film was estimated ranging between $\approx 1.00 - 2.00 \mu\text{m}$ and confirming the irregular film surface. The micrograph of Figure 5 (b) is representative of some regions observed in the exposed inside film structure (region Z1), in which were distinguished agglomerates assigned to TiO_2 NPs (region Z2) occluded on poly[1] matrix, on the basis of EDS analysis (Figure 5 (c)). These revealed different compositions for regions Z1 and Z2: in region Z1 the elements characteristic of poly[1] and its ClO_4^- counter ion (Ni, O, C and Cl) were detected and in region Z2 there is also Ti from the TiO_2 NPs.

The characterization of $\text{TiO}_2@\text{poly}[1]_r$ nanocomposite by XPS shows Ni, C, N, O and Cl, from poly[1] and species incorporated upon redox cycling (ClO_4^- and solvent). Observed and calculated surface atomic percentages and atom ratios are summarised in Table 1, along with data for poly[1] for comparison.

| |
|---------|
| Table 1 |
|---------|

The atomic ratios of the nanocomposite before redox switching are similar to those of pristine poly[1]²⁸ and the slightly larger ratios in comparison to the theoretical values ($\text{N}/\text{Ni}_{\text{theoretical}} = \text{O}/\text{Ni}_{\text{theoretical}} = 2.0$ and $\text{Cl}/\text{Ni}_{\text{theoretical}} = 0.0$) are assigned to the trapping of the TiO_2 NPs and some $\text{LiClO}_4/\text{CH}_3\text{CN}$ on poly[1] matrix, during electropolymerization.

After redox switching in $\text{LiClO}_4/\text{CH}_3\text{CN}$, the nanocomposite film shows a significant increase in Cl/Ni and O/Ni ratios, as a consequence of redox-driven accumulation of ClO_4^- and solvent in the film. The increase in Cl/Ni and O/Ni atomic

ratios was larger for TiO₂@poly[1]_r than for poly[1]. Redox switching in LiClO₄/PC also led to increases of similar magnitude in Cl/Ni and O/Ni atomic ratios for the nanocomposite and pristine films.

The high-resolution XPS spectra obtained for both films before and after redox switching in LiClO₄/CH₃CN and LiClO₄/PC are shown in Figures from S10 to S14, in SI.

The XPS spectra in the C1s region (Figure S10) were deconvoluted into four peaks: a main peak at 284.6 eV attributed to aromatic and aliphatic carbons of the *salen* ligand, a peak at 285.9-286.0 eV assigned to carbon bound to oxygen and nitrogen in the *salen* moiety, a peak at 286.9-287.0 eV ascribed to C≡N or to C=O from CH₃CN or PC, respectively, and a peak at 289.3-290.0 eV assigned to a shake-up satellite due to π - π^* transitions in the ligand.³⁵

The film N1s spectra before and after redox switching in LiClO₄/CH₃CN (Figure S11 (a), (a'), (b) and (b')) were deconvoluted into four peaks, at 399.4-399.5 eV, 400.2-400.4 eV, 401.0-401.5 eV and 403.4-403.6 eV attributed, respectively, to the nitrogen atoms of the ligand system (N=C and N-C bonds), N≡C of the occluded CH₃CN and to a shake-up phenomenon.³⁵ In the nanocomposite spectra, the first peak also has a contribution from N-Ti and N-O-Ti bonds from TiO₂ NPs. In the spectra of films after redox cycling in LiClO₄/PC (Figure S11 (c) and (c')), the peak at 401.0-401.5 eV was not identified, once the solvent was changed for PC, and all others remain similar.

The O1s spectra of nanocomposite films before redox switching (Figure S12 (a')) were deconvoluted into three peaks (531.2, 532.5 and 533.4 eV). The former is assigned to the oxygen of the *salen* coordination sphere³⁵ and to O-Ti bonds, while the last two are ascribed to trapped ClO₄⁻ with different local environments and to -OH groups from TiO₂ NPs. In the spectrum of the nanocomposite after redox switching in LiClO₄/CH₃CN (Figure S12 (b')), we observe a peak at 531.7 eV (O of *salen* coordination sphere and O-

Ti), along with a large peak at 533.3 eV ascribed to –OH groups from TiO₂ and to larger amounts of ClO₄⁻, trapped in the polymeric film as the charge compensating anion. For the nanocomposite after redox cycling in LiClO₄/PC (Figure S12 (c')), beyond the two peaks at 531.2 and 532.5 eV (similarly to the redox in LiClO₄/CH₃CN), we observe an additional peak at 533.5 eV, assigned to O-C bonds in entrapped PC.

In the Cl2p spectra (Figure S13) two peaks are observed (at 208.1-208.6 eV and 209.7-210.2 eV). These are assigned to Cl2p_{3/2} and Cl2p_{1/2} associated with ClO₄⁻ trapped in the film (see above).

The Ni2p region (Figure S14) shows the characteristic peaks of Ni in a formal +2 oxidation state, which are attributed to Ni2p_{3/2} (855.2-855.4 eV), Ni2p_{3/2} satellite (860.1-860.7 eV), Ni2p_{1/2} (872.4-872.6 eV) and Ni2p_{1/2} satellite (877.3-877.8 eV).³⁵

In this XPS analyses, Ti was not detected. We rationalise this by recognizing that XPS is (very) surface specific, in which case the failure to observe Ti indicates that the NPs are not present (effectively at undetectably low concentration) or are sub-surface within films much thicker than their diameter. To test this hypothesis, a subsequent XPS experiment was performed, in which the nanocomposite surface was subject to erosion by ion bombardment. The spectra revealed new peaks in the BE range 455 – 470 eV typical of Ti species. Deconvolution of the XPS spectrum in this region (Figure S15) was yielded two peaks (at 459.9 eV and 465.5 eV), assigned to Ti2p_{3/2} and Ti2p_{1/2}, respectively; the peak separation ($\Delta = 5.6$ eV), is typical of Ti in a TiO₂ matrix.⁴² These observations confirm the successful preparation of the TiO₂@poly[1]_r nanocomposite.

In Figure S16 is shown the XRD pattern obtained for TiO₂@poly[1]_r nanocomposite film, along with the TiO₂_400 NPs and original poly[1] film. In the TiO₂@poly[1]_r and poly[1] diffractograms are observed several peaks at $2\theta = 39.8, 46.1$ and 67.4° , which are marked with *, that are attributed to Pt substrate used in films

electrodeposition for XRD analysis, and the peak observed at $2\theta \approx 20.2^\circ$ in the $\text{TiO}_2@\text{poly}[1]_r$ diffractogram that is assigned to LiClO_4 (supporting electrolyte) occluded in the nanocomposite matrix. Furthermore, in the nanocomposite diffractogram is clearly detected a new peak at $2\theta = 25.2^\circ$, not observed in the poly[1] diffractogram, that is assigned to the most intense diffraction peak A(101)/B(120)(111) of TiO_2 NPs, confirming their incorporation in the Ni-*salen* film. The other low intense peaks due to TiO_2 crystalline phases are not clearly identified in the nanocomposite diffractogram, due to low quantity of TiO_2 compared to that of the polymer film, but they should have some contribution for remaining XRD peaks.

***In situ* UV-Vis spectroscopy**

The absolute UV-Vis spectra acquired during the oxidation of $\text{TiO}_2@\text{poly}[1]$ nanocomposites (with 5 wt.% of TiO_2 NPs) are depicted in Figure 6 (b) and (c); the equivalent spectra for pristine poly[1] film are presented in Figure 6 (a), for comparison. The spectra obtained during film reduction show the inverse behaviour and were omitted for simplicity.

Figure 6

Both nanocomposite spectra show four electronic bands, as does the spectrum of the poly[1] film. Figure S17 shows the differential spectra, in which responses at selected potentials were used as reference, highlighting the electronic band dependence on potential. These spectra, as well as the absorbance vs. potential (*Abs* vs. *E*) profiles at selected wavelengths (Figures 6 (a') and (b') and (c')), indicated that the nanocomposites present three main band profiles, like the pristine film²⁸ and similar to other

poly[M(*salen*)] films:^{35,36} (i) a band at low wavelength ($\lambda = 327$ nm) whose intensities decrease monotonically with increasing potential, (ii) two bands, at $\lambda = 396-398$ nm and at $\lambda = 839-850$ nm, whose intensities increase until $E = 0.8-0.9$ V and thereafter decrease until the end of the positive half cycle, and (iii) a band at $\lambda = 505-509$ nm, whose intensity increase monotonically with potential from $E = 0.8-0.9$ V until the end of the positive half scan.

The energies of the electronic bands observed for all films are summarised in Table 2, together with the molar extinction coefficients, ε , estimated from the slopes of *Abs* vs. *Q* plots (Figure S18) using Equation 2.

| |
|---------|
| Table 2 |
|---------|

The ε -values obtained for nanocomposites are typical of electronic transitions between states with large contribution from ligand, which is consistent with the ligand-based film oxidation, as proposed for poly[1]²⁸ and other similar poly[Ni(*salen*)] films.^{35,36} Using the polaronic model^{35,36} and considering that electronic bands with similar *Abs* vs. *E* profiles are associated with the same charge carriers, the following band assignment can be proposed, assuming that the intergap states are not symmetrically positioned: (i) the band at $\lambda = 327$ nm is attributed to the intervalence transition (band gap, $E_g = 3.80$ eV), (ii) the band at $\lambda = 396-397$ nm (3.14-3.13 eV) is assigned to transitions from the valence band to the antibonding polaron level and (iii) the band at $\lambda = 839-840$ nm (1.48 eV) corresponds to transitions from the valence band to the bonding polaron level (or between polaron levels). The band at $\lambda = 505-509$ nm (2.44-2.46 eV), with its different *Abs* vs. *E* profiles, is attributed to charge transfer (CT) transitions between the metal and the oxidized ligand.^{35,36} Furthermore, the bands observed in spectra

of nanocomposites and pristine films have similar energies, which indicate that the electronic structure of poly[1] was not substantially changed by the incorporation of TiO₂ NPs.

The ϵ -values for the nanocomposite electronic bands are also similar to those of the pristine film, except for the band assigned to CT transitions at $\lambda = 505\text{-}506$ nm (2.44-2.46 eV). For this band, the ϵ -value decreases significantly from the pristine to the nanocomposite films. The ϵ -value decrease slightly (by 3.6 %, from $\epsilon = 12.2 \times 10^3$ to 11.8×10^3 mol⁻¹ dm³ cm⁻¹) for the TiO₂@poly[1]_s nanocomposite, and somewhat more significantly (by 16.2 %, from $\epsilon = 12.2 \times 10^3$ vs. 10.2×10^3 mol⁻¹ dm³ cm⁻¹) for the TiO₂@poly[1]_r nanocomposite. Overall, since the CT bands are associated with less stable oxidised states of poly[1], the decrease in ϵ indicates an increase in nanocomposite resistance to over-oxidation upon TiO₂ incorporation, particularly for TiO₂@poly[1]_r. We may speculate that TiO₂ incorporation into poly[1] matrix changes the packing of polymer strands, creating a more porous structure that may facilitate ion/solvent mobility required for charge compensation during redox process, anticipating high electrochemical stability (see below); simultaneously its semiconductor properties may also facilitate electronic conduction between the polymer strands. Consequently, the overall conducting properties will be better in the nanocomposite decreasing the tendency to ligand overoxidation. At a finer level of detail, the different results amongst variously prepared TiO₂@poly[1] nanocomposites indicate sensitivity to synthetic protocols.

Electrochromic properties

The outcomes of the more fundamentally oriented spectroelectrochemical studies now prompt the study of the EC properties of TiO₂@poly[1]_r, with those of the original film used as a benchmark.

Extended electrochemical stability for a representative $\text{TiO}_2@\text{poly}[1]_r$ nanocomposite film ($\Gamma = 270 \text{ nmol cm}^{-2}$) was evaluated by the chronoamperometric response to *ca.* 10,000 consecutive redox cycles between the yellow and green states. The chronoamperograms obtained are depicted in Figure 7 (a) and show that at the end of 11 days (9504 electrochemical cycles), the nanocomposite film had a charge loss of only 7.3 %, while the original film ($\Gamma = 184 \text{ nmol cm}^{-2}$), in the same experimental conditions, lost 13.7%; significantly, formation of the nanocomposite cut the charge loss by a factor of approximately two. We attribute this to a combination of electronic (electron donor-acceptor interaction of the TiO_2 NPs and poly[1]) and structural (modified hybrid architecture) factors promoted by the intimate contact of the NPs and CP.²¹

Figure 7

The response times (Figure 7 (b)) reveal very similar responses between the nanocomposite and the pristine film: during the 19th cycle, the nanocomposite needs $\tau = 29 \text{ s}$ to change colour between green and yellow and $\tau = 24 \text{ s}$ to return to green, while poly[1] needs $\tau = 29$ and 20 s , respectively. These response times remains almost unchanged during several cycles, as demonstrate by the times obtained at the 3000th cycle ($\tau = 18 - 30 \text{ s}$).

The optical contrast ($\Delta T \%$), optical density change and colouration efficiency were evaluated through the monitoring of a similar chronoamperometry experiment by *in situ* UV-Vis spectroscopy, focusing on the optical response at $\lambda = 750 \text{ nm}$. Figure 7 (c) shows data for representative nanocomposite film ($\Gamma = 108 \text{ nmol cm}^{-2}$). Numerical outcomes are summarised in Table 3, as well as for pristine poly[1] film ($\Gamma = 95.3 \text{ nmol cm}^{-2}$) for reference.

| |
|---------|
| Table 3 |
|---------|

The ΔT values, measured considering the full optical change between yellow and green, slightly decrease from the pristine poly[1] film ($\Delta T = 46.3\%$) to $\text{TiO}_2@\text{poly}[1]_r$ ($\Delta T = 43.4\%$). The ΔOD values slightly increase from $\Delta OD = 0.40$ in poly[1] to $\Delta OD = 0.48$ in $\text{TiO}_2@\text{poly}[1]_r$, representing an improvement of 16.7%. Moving to the colouration efficiency of nanocomposite, which effectively normalises for population (via associated redox charge, $Q_d = 5.45$ vs. 4.53 mC cm^{-2}), the values are practically indistinguishable for the nanocomposite and the pristine film ($\eta = 87.5$ vs. $87.7 \text{ cm}^2 \text{ C}^{-1}$).

To summarize, the incorporation of TiO_2 NPs into the poly[1] matrix yields material with two crucial practical advantages, namely higher ΔOD and excellent electrochemical stability in LiClO_4/PC . This is consistent with literature reports for nanocomposites of TiO_2 NPs and PANI^{20,24,25} or PEDOT:PSS,¹³ both of which showed faster and better optical modulation and superior cycling stability to the corresponding pristine CPs.

The EC property evaluation was complemented by a colorimetric study, considering the importance of the colour for practical applications of EC materials. The CIELAB coordinate values (L^* , a^* and b^*) and colour difference ΔE^* between different oxidation states for nanocomposite and pristine films are summarised in Table 4. The b^* vs. a^* plot (Figure 8) shows that at $E = 0.0 \text{ V}$, the colour of both films is situated in the yellow-red quadrant, at high b^* coordinates, indicating a predominant yellow colour. At $E = 0.7 \text{ V}$, the coordinates are dislocated to yellow-green quadrant, at low a^* values, reflecting a green colour. These results are in agreement with the photographs shown in Figure 4. At $E = 1.3 \text{ V}$, the coordinates are localized in the yellow-red quadrant, at low a^* and b^* values, reflecting a colour between green and red, but lighter than the real

colour observed (russet). This divergence is explained by the low stability of the films at high potential values: after the removal of the electrical stimulus ($E = 1.3$ V), the colour of films decays rapidly from russet to green; however, as the colorimetric study is *ex situ*, some uncertainty is associated with the CIELAB coordinates determined at $E = 1.3$ V.

| |
|---------|
| Table 4 |
|---------|

| |
|----------|
| Figure 8 |
|----------|

For the colour change yellow-green, the nanocomposite film showed a slightly greater EC response ($\Delta E^* = 54.9$) than poly[1], which is in agreement with the obtained ΔOD values. For the colour change green-russet, the ΔE^* obtained was lower for the nanocomposite.

CONCLUSIONS

The results showed that poly[1] was successfully electropolymerized in the presence of TiO₂ NPs spherically shaped with 9.7 ± 1.1 nm and containing both anatase (66.0 ± 0.4 vol.%) and brookite (34.0 ± 0.4 vol.%) phases.

Pristine and nanocomposite films showed similar voltammetric responses, with the nanocomposite films showing higher electroactive surface coverages. Moreover, the increase of I is most significant for nanocomposite films electropolymerized at $v = 0.020$ mV s⁻¹ and rises with TiO₂ loading from 5 and 15 wt.%, but decreasing for TiO₂ loading of 25 wt.% (in the deposition feedstock); we suggest that high TiO₂ content can hinder polymer electrodeposition. The incorporation of TiO₂ NPs into the poly[1] matrix was confirmed by SEM and XPS. The UV-Vis spectra show similar electron band profiles

and energies between pristine and nanocomposites films, but lower ε -values were determined for the CT band of the nanocomposites, suggesting higher stability for ligand oxidation.

The TiO₂@poly[1]_r nanocomposite showed excellent electrochemical stability, with a charge loss of only 7.3 % after \approx 10,000 redox cycles, which represents halving of the charge loss in comparison to a pristine poly[1] film. The Δ OD also showed an increase of 16.7 % for nanocomposite films. These results clearly show the advantage of nanocomposite preparation in the pursue for a solution to improve the EC properties of the pristine poly[1].

SUPPORTING INFORMATION

Results and discussion of TiO₂ NPs characterization (XRD, TEM, XPS, FTIR and UV-Vis); Voltammetric responses and peak potential values, XPS spectra, XRD diffractograms, differential UV-Vis spectra and *Abs* vs. *Q* plots for the nanocomposite and pristine films.

ACKNOWLEDGMENTS

The work was funded by European Union and Fundação para a Ciência e a Tecnologia (FCT)/MEC under FEDER funds (POCI/01/0145/FEDER/007265) and Program PT2020 (UID/QUI/50006/2013). MN thanks FEDER funds POCI/01/0145/FEDER/007265 and PT2020 UID/QUI/50006/2013 for her post-doctoral grant.

ORCID ID's

Marta Nunes: orcid.org/0000-0002-0460-451X

Cosme Moura: orcid.org/0000-0001-7760-0504

A.R. Hillman: orcid.org/0000-0003-1868-5717

Cristina Freire: orcid.org/0000-0003-1753-8678

REFERENCES

- (1) Dziewonski, P. M.; Grzeszczuk, M. Towards TiO₂-conducting polymer hybrid materials for lithium ion batteries. *Electrochim. Acta* **2010**, *55*, 3336-3347.
- (2) Takagi, S.; Makuta, S.; Veamatahau, A.; Otsuka, Y.; Tachibana, Y. Organic/inorganic hybrid electrochromic devices based on photoelectrochemically formed polypyrrole/TiO₂ nanohybrid films. *J. Mater. Chem.* **2012**, *22*, 22181-22189.
- (3) Janaky, C.; de Tacconi, N. R.; Chanmanee, W.; Rajeshwar, K. Bringing Conjugated Polymers and Oxide Nanoarchitectures into Intimate Contact: Light-Induced Electrodeposition of Polypyrrole and Polyaniline on Nanoporous WO₃ or TiO₂ Nanotube Array. *Journal of Physical Chemistry C* **2012**, *116*, 19145-19155.
- (4) Abaci, S.; Nessark, B.; Riahi, F. Preparation and characterization of polyaniline+TiO₂ composite films. *Ionics* **2014**, *20*, 1693-1702.
- (5) Ma, D. Y.; Shi, G. Y.; Wang, H. Z.; Zhang, Q. H.; Li, Y. G. Controllable growth of high-quality metal oxide/conducting polymer hierarchical nanoarrays with outstanding electrochromic properties and solar-heat shielding ability. *J. Mater. Chem. A* **2014**, *2*, 13541-13549.
- (6) Yang, L.; Zhang, J. B.; Shen, Y.; Park, B. W.; Bi, D. Q.; Haggman, L.; Johansson, E. M. J.; Boschloo, G.; Hagfeldt, A.; Vlachopoulos, N.; Snedden, A.; Kloo, L.; Jarboui, A.; Chams, A.; Perruchot, C.; Jouini, M. New Approach for Preparation of Efficient Solid-State Dye-Sensitized Solar Cells by Photoelectrochemical Polymerization in Aqueous Micellar Solution. *J. Phys. Chem. Lett.* **2013**, *4*, 4026-4031.
- (7) Sidhu, N. K.; Rastogi, A. C., Vertically aligned ZnO nanorod core-polypyrrole conducting polymer sheath and nanotube arrays for electrochemical supercapacitor energy storage. *Nanoscale Res. Lett.* **2014**, *9*, 453.
- (8) Gottam, R.; Srinivasan, P. One-step oxidation of aniline by peroxotitanium acid to polyaniline-titanium dioxide: A highly stable electrode for a supercapacitor. *J. Appl. Polym. Sci.* **2015**, *132*, 41711.
- (9) Arjomandi, J.; Mossa, N. K. I.; Jaleh, B. Electrochemical Synthesis and *In Situ* Spectroelectrochemistry of Conducting NMPy-TiO₂ and ZnO Polymer Nanocomposites for Li Secondary Battery Applications. *J. Appl. Polym. Sci.* **2015**, *132*, 41526.
- (10) Hidalgo, D.; Bocchini, S.; Fontana, M.; Saracco, G.; Hernandez, S. Green and low-cost synthesis of PANI-TiO₂ nanocomposite mesoporous films for photoelectrochemical water splitting. *RSC Adv.* **2015**, *5*, 49429-49438.
- (11) Zhu, J.; Liu, X. Q.; Wang, X. H.; Huo, X. H.; Yan, R. Preparation of polyaniline-TiO₂ nanotube composite for the development of electrochemical biosensors. *Sens. Actuator B-Chem.* **2015**, *221*, 450-457.

- (12) Cai, G. F.; Tu, J. P.; Zhou, D.; Zhang, J. H.; Wang, X. L.; Gu, C. D. Dual electrochromic film based on WO₃/polyaniline core/shell nanowire array. *Sol. Energy Mater. Sol. Cells* **2014**, *122*, 51-58.
- (13) Lu, J. L.; Song, H.; Li, S. N.; Wang, L.; Han, L.; Ling, H.; Lu, X. H. A poly(3,4-ethylenedioxythiophene):poly(styrene sulfonic acid)/titanium oxide nanocomposite film synthesized by sol-gel assisted electropolymerization for electrochromic application. *Thin Solid Films* **2015**, *584*, 353-358.
- (14) Liu, S. P.; Zhang, X. T.; Sun, P. P.; Wang, C. H.; Wei, Y. A.; Liu, Y. C. Enhanced electrochromic properties of a TiO₂ nanowire array via decoration with anatase nanoparticles. *J. Mater. Chem. C* **2014**, *2*, 7891-7896.
- (15) Hajzeri, M.; Perse, L. S.; Kozelj, M.; Orel, B.; Vuk, A. S. Structural investigation of ormolytes for EC devices: IR spectroscopic characterization and relation between viscoelastic properties, conductivity and optical modulation. *Sol. Energy Mater. Sol. Cells* **2015**, *139*, 51-64.
- (16) Mortimer, R. J. Electrochromic Materials. In *Annual Review of Materials Research, Vol 41*, Clarke, D. R.; Fratzi, P., Eds. Annual Reviews: Palo Alto, 2011; Vol. 41, pp 241-268.
- (17) Beverina, L.; Pagani, G. A.; Sassi, M. Multichromophoric electrochromic polymers: colour tuning of conjugated polymers through the side chain functionalization approach. *Chem. Commun.* **2014**, *50*, 5413-5430.
- (18) Shankar, S.; Lahav, M.; van der Boom, M. E. Coordination-Based Molecular Assemblies as Electrochromic Materials: Ultra-High Switching Stability and Coloration Efficiencies. *J. Am. Chem. Soc.* **2015**, *137*, 4050-4053.
- (19) Yassin, A.; Ocafrain, M.; Blanchard, P.; Mallet, R.; Roncali, J. Synthesis of Hybrid Electroactive Materials by Low-Potential Electropolymerization of Gold Nanoparticles Capped with Tailored EDOT-Thiophene Precursor Units. *ChemElectroChem* **2014**, *1*, 1312-1318.
- (20) Xia, X. H.; Chao, D. L.; Qi, X. Y.; Xiong, Q. Q.; Zhang, Y. Q.; Tu, J. P.; Zhang, H.; Fan, H. J. Controllable Growth of Conducting Polymers Shell for Constructing High-Quality Organic/Inorganic Core/Shell Nanostructures and Their Optical-Electrochemical Properties. *Nano Lett.* **2013**, *13*, 4562-4568.
- (21) Janaky, C.; Rajeshwar, K. The role of (photo)electrochemistry in the rational design of hybrid conducting polymer/semiconductor assemblies: From fundamental concepts to practical applications. *Prog. Polym. Sci.* **2015**, *43*, 96-135.
- (22) Eren, E.; Celik, G.; Uygun, A.; Tabaciaraova, J.; Omastova, M. Synthesis of poly(3,4-ethylenedioxythiophene)/titanium dioxide nanocomposites in the presence of surfactants and their properties. *Synth. Met.* **2012**, *162*, 1451-1458.
- (23) Ngaboyamahina, E.; Cachet, H.; Pailleret, A.; Sutter, E. M. M. Photo-assisted electrodeposition of an electrochemically active polypyrrole layer on anatase type titanium dioxide nanotube arrays. *Electrochim. Acta* **2014**, *129*, 211-221.

- (24) Cai, G. F.; Tu, J. P.; Zhou, D.; Zhang, J. H.; Xiong, Q. Q.; Zhao, X. Y.; Wang, X. L.; Guts, C. D. Multicolor Electrochromic Film Based on TiO₂@Polyaniline Core/Shell Nanorod Array. *Journal of Physical Chemistry C* **2013**, *117*, 15967-15975.
- (25) Xiong, S. X.; Phua, S. L.; Dunn, B. S.; Ma, J.; Lu, X. H. Covalently Bonded Polyaniline-TiO₂ Hybrids: A Facile Approach to Highly Stable Anodic Electrochromic Materials with Low Oxidation Potentials. *Chem. Mat.* **2010**, *22*, 255-260.
- (26) Pinheiro, C.; Parola, A. J.; Pina, F.; Fonseca, J.; Freire, C. Electrocolorimetry of electrochromic materials on flexible ITO electrodes. *Sol. Energy Mater. Sol. Cells* **2008**, *92*, 980-985.
- (27) Branco, A.; Pinheiro, C.; Fonseca, J.; Tedim, J.; Carneiro, A.; Parola, A. J.; Freire, C.; Pina, F. Solid-State Electrochromic Cells Based on M(*salen*)-Derived Electroactive Polymer Films. *Electrochim. Solid State Lett.* **2010**, *13*, J114-J118.
- (28) Nunes, M.; Araujo, M.; Fonseca, J.; Moura, C.; Hillman, R.; Freire, C. High-Performance Electrochromic Devices Based on Poly Ni(*salen*)-Type Polymer Films. *ACS Appl. Mater. Interfaces* **2016**, *8*, 14231-14243.
- (29) Huang, B. R.; Lin, T. C.; Liu, Y. M. WO₃/TiO₂ core-shell nanostructure for high performance energy-saving smart windows. *Sol. Energy Mater. Sol. Cells* **2015**, *133*, 32-38.
- (30) Freire, C.; de Castro, B. Spectroscopic characterisation of electrogenerated nickel(III) species. Complexes with N₂O₂ Schiff-base ligands derived from salicylaldehyde. *J. Chem. Soc.-Dalton Trans.* **1998**, *9*, 1491-1497.
- (31) Mahshid, S.; Askari, M.; Ghamsari, M. S. Synthesis of TiO₂ nanoparticles by hydrolysis and peptization of titanium isopropoxide solution. *J. Mater. Process. Technol.* **2007**, *189*, 296-300.
- (32) Silva, E.; La Porta, F. A.; Liu, M. S.; Andres, J.; Varela, J. A.; Longo, E. A relationship between structural and electronic order-disorder effects and optical properties in crystalline TiO₂ nanomaterials. *Dalton Trans.* **2015**, *44*, 3159-3175.
- (33) Chen, C. C.; Hu, S. H.; Fu, Y. P. Effects of surface hydroxyl group density on the photocatalytic activity of Fe³⁺-doped TiO₂. *J. Alloy. Compd.* **2015**, *632*, 326-334.
- (34) Choi, M.; Yong, K. A facile strategy to fabricate high-quality single crystalline brookite TiO₂ nanoarrays and their photoelectrochemical properties. *Nanoscale* **2014**, *6*, 13900-13909.
- (35) Fonseca, J.; Tedim, J.; Biernacki, K.; Magalhaes, A. L.; Gurman, S. J.; Freire, C.; Hillman, A. R. Structural and electrochemical characterisation of Pd(*salen*)-type conducting polymer films. *Electrochim. Acta* **2010**, *55*, 7726-7736.
- (36) Tedim, J.; Patricio, S.; Fonseca, J.; Magalhaes, A. L.; Moura, C.; Hillman, A. R.; Freire, C. Modulating spectroelectrochemical properties of Ni(*salen*) polymeric films at molecular level. *Synth. Met.* **2011**, *161*, 680-691.

- (37) Dale, S. M.; Glidle, A.; Hillman, A. R. Spectroelectrochemical Observation of poly(benzo-c-thiophene) n-doping and p-doping. *J. Mater. Chem.* **1992**, *2*, 99-104.
- (38) Schott, M.; Lorrmann, H.; Szczerba, W.; Beck, M.; Kurth, D. G. State-of-the-art electrochromic materials based on metallo-supramolecular polymers. *Sol. Energy Mater. Sol. Cells* **2014**, *126*, 68-73.
- (39) Beaujuge, P. M.; Reynolds, J. R. Color Control in pi-Conjugated Organic Polymers for Use in Electrochromic Devices. *Chem. Rev.* **2010**, *110*, 268-320.
- (40) Pinto, T.V, Fernandes, D.M., Pereira, C., Guedes, A., Blanco, G., Pintado, J.M., Pereira, M.F.R., Freire, C. Lanthano phosphomolybdate-decorated silica nanoparticles: novel hybrid materials with photochromic properties. *Dalton Trans.* **2015**, *44*, 4582-4593.
- (41) Lin, C. K.; Tseng, S. C.; Cheng, C. H.; Chen, C. Y.; Chen, C. C. Electrochromic performance of hybrid tungsten oxide films with multiwalled-CNT additions. *Thin Solid Films* **2011**, *520*, 1375-1378.
- (42) Cheng, J.; Chen, J.; Lin, W.; Liu, Y.; Kong, Y. Improved visible light photocatalytic activity of fluorine and nitrogen co-doped TiO₂ with tunable nanoparticle size. *Applied Surface Science* **2015**, *332*, 573-580.

Figures

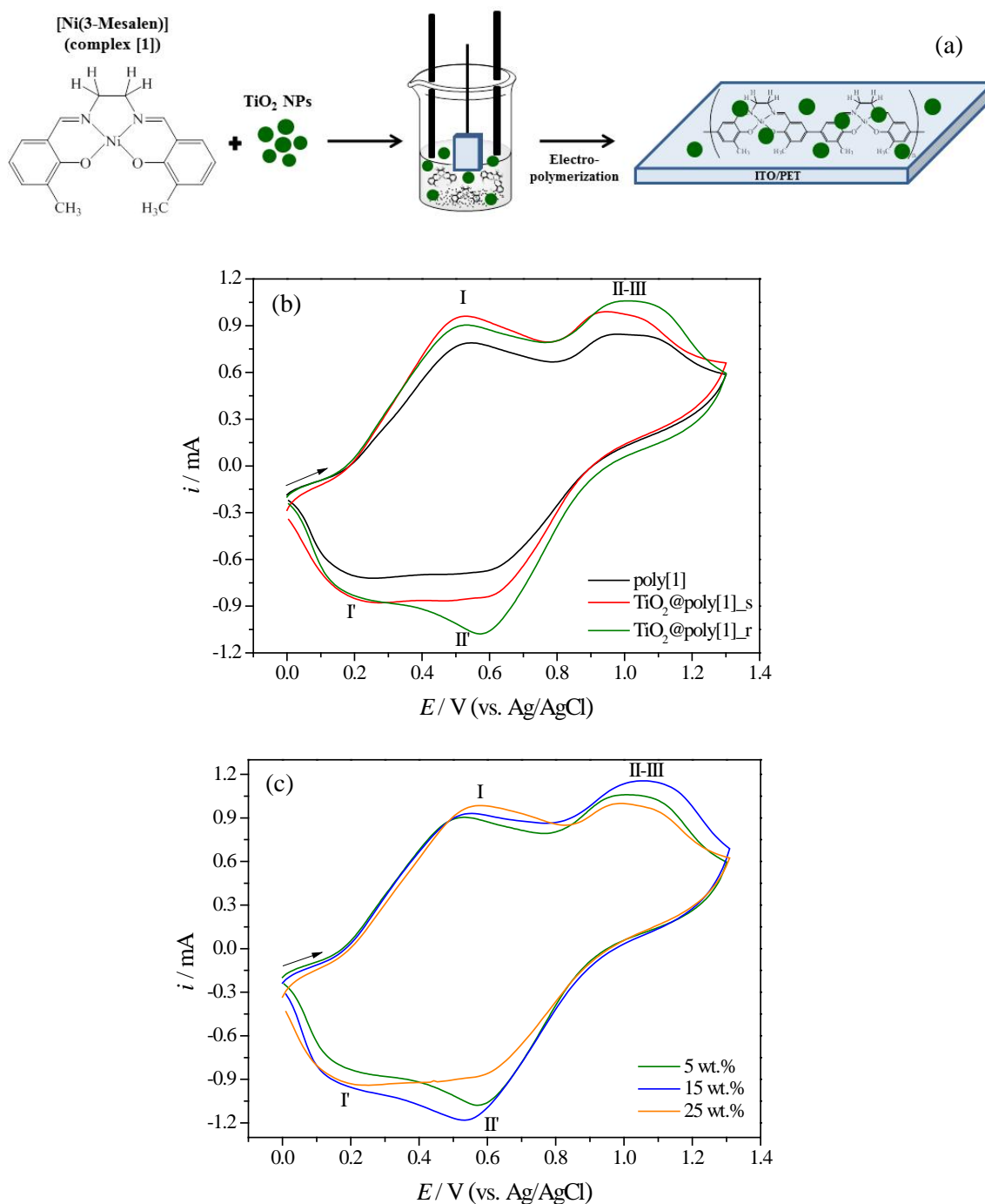


Figure 1. (a) Schematic representation of the complex [1] electro-polymerization in the presence of TiO_2 NPs. Cyclic voltammograms obtained during the 10th electrodeposition cycles of (b) poly[1], TiO_2 @poly[1]_s and TiO_2 @poly[1]_r (with 5 wt.% of TiO_2 loading) and (c) TiO_2 @poly[1]_r with 5, 15 and 25 wt.% of TiO_2 loading. Solution: 1.0 mmol dm⁻³ of monomer in 0.1 mol dm⁻³ $\text{LiClO}_4/\text{CH}_3\text{CN}$ supporting electrolyte. Scan rate, $\nu = 0.020 \text{ V s}^{-1}$.

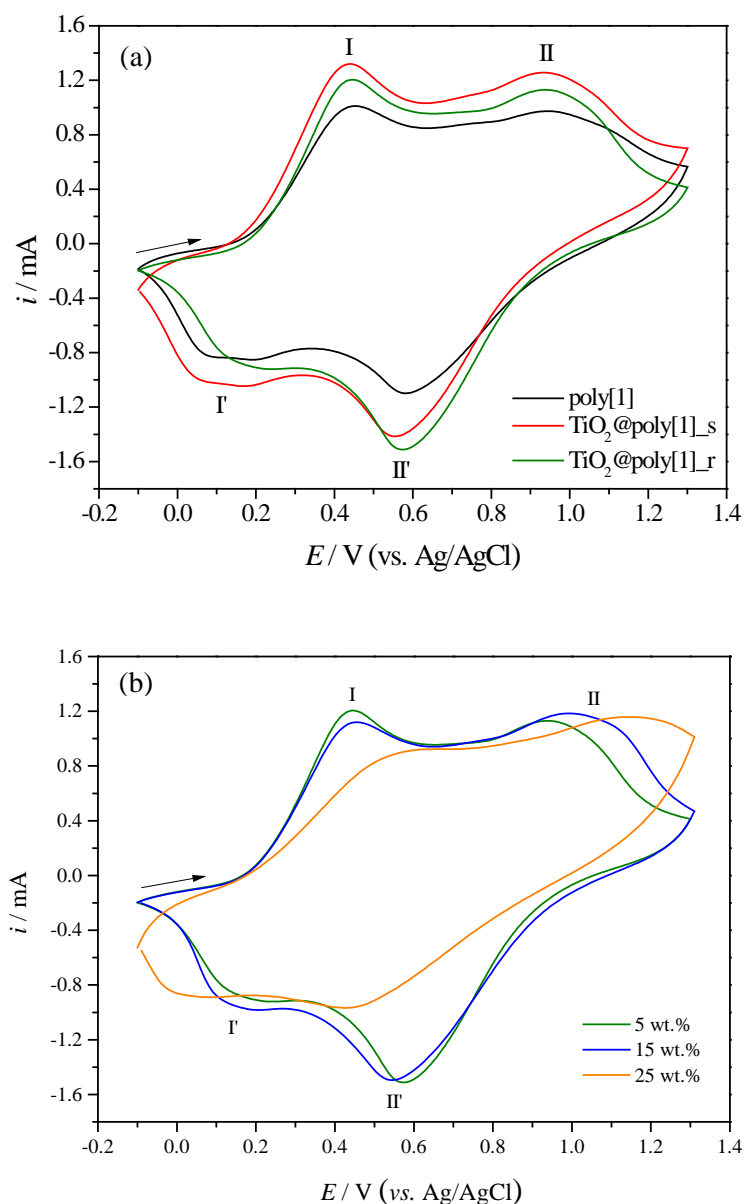


Figure 2. Cyclic voltammograms obtained during the 5th scan of redox switching of films previously electrodeposited at $\nu = 0.020 \text{ V s}^{-1}$: (a) poly[1], TiO₂@poly[1]_s and TiO₂@poly[1]_r (with 5 wt.% of TiO₂ loading) and (b) TiO₂@poly[1]_r with 5, 15 and 25 wt.% of TiO₂ loading. Solution: $0.1 \text{ mol dm}^{-3} \text{ LiClO}_4/\text{CH}_3\text{CN}$ supporting electrolyte. Scan rate, $\nu = 0.020 \text{ V s}^{-1}$.

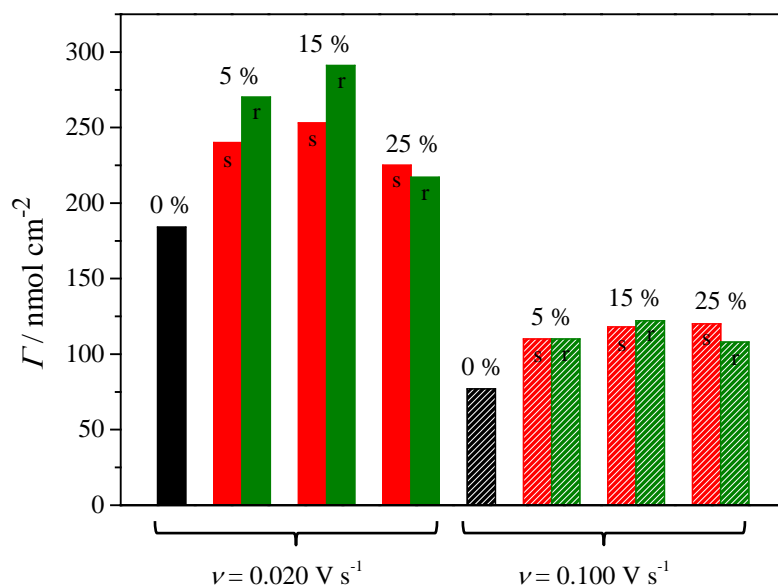


Figure 3. Electroactive surface coverage, Γ / nmol cm⁻², for films prepared by different protocols, using different TiO₂ loadings (indicated in figure) and electrodeposition scan rates ($\nu = 0.020$ V s⁻¹ (solid columns) or $\nu = 0.100$ V s⁻¹ (hatched columns)). In redox switching, $\nu = 0.010$ V s⁻¹. Black columns correspond to poly[1], red columns to TiO₂@poly[1]_s (labelled “s”) and green columns TiO₂@poly[1]_r (labelled “r”).

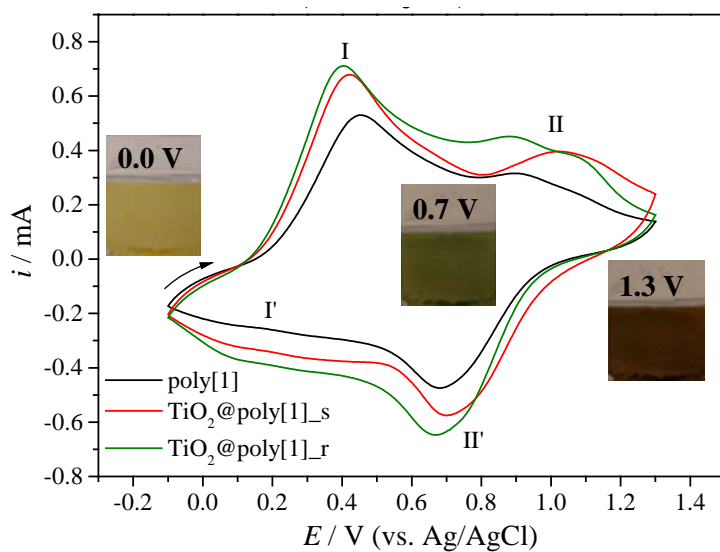


Figure 4. CVs obtained during the 3rd redox cycle of the poly[1] ($\Gamma = 184 \text{ nmol cm}^{-2}$) and $\text{TiO}_2@poly[1]$ (with 5 wt.% of TiO_2 loading, electropolymerized at $\nu = 0.020 \text{ V s}^{-1}$, $\Gamma = 240$ or 270 nmol cm^{-2}) in LiClO_4/PC 0.1 mol dm^{-3} , at the scan rate of $\nu = 0.010 \text{ V s}^{-1}$; the insets are photographs of the polymeric film in different oxidation states.

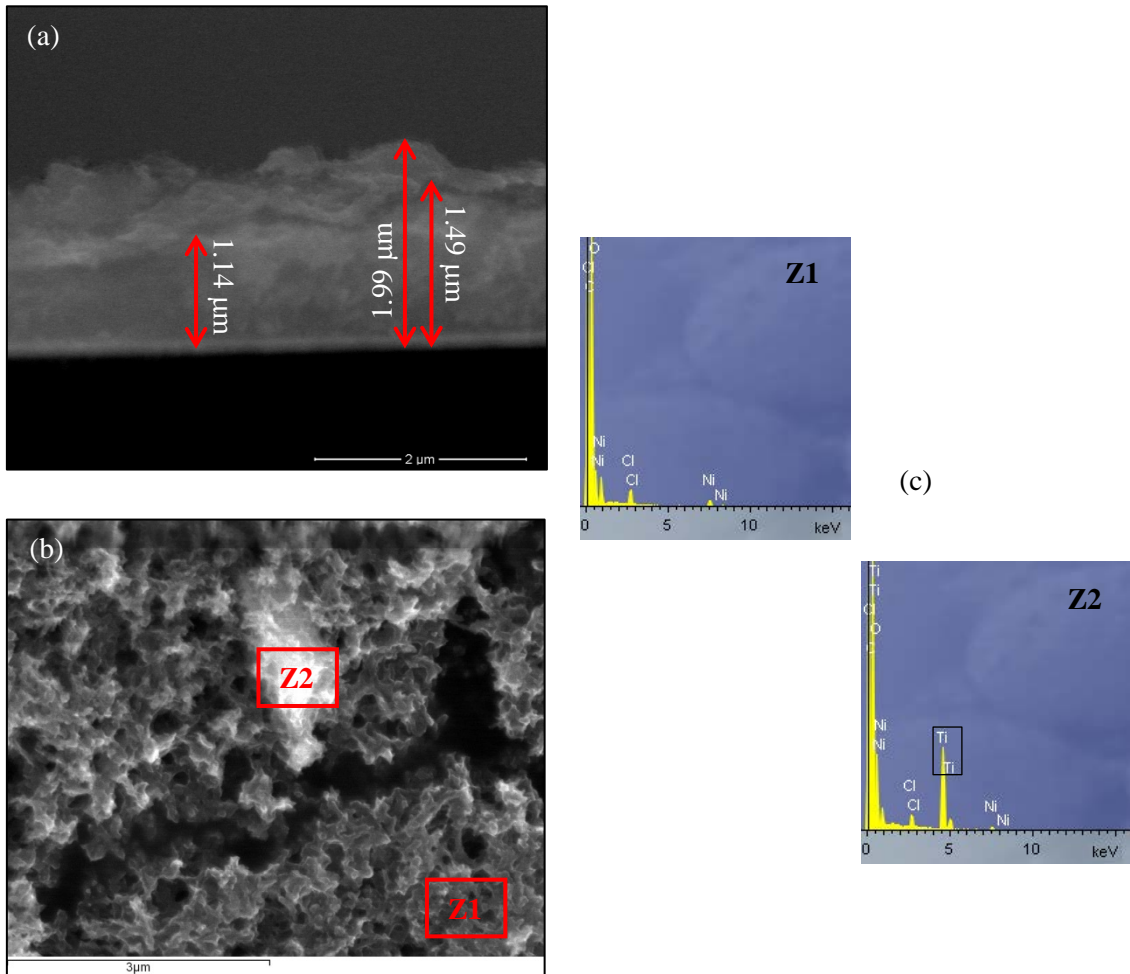


Figure 5. Scanning electron micrographs of TiO_2 @poly[1]_r nanocomposite film in (a) cross-section and (b) internal plan (plane view, magnifications of 50 000 and 20 000 times, respectively; see scale bars); (c) EDS spectra at zones specified in (b).

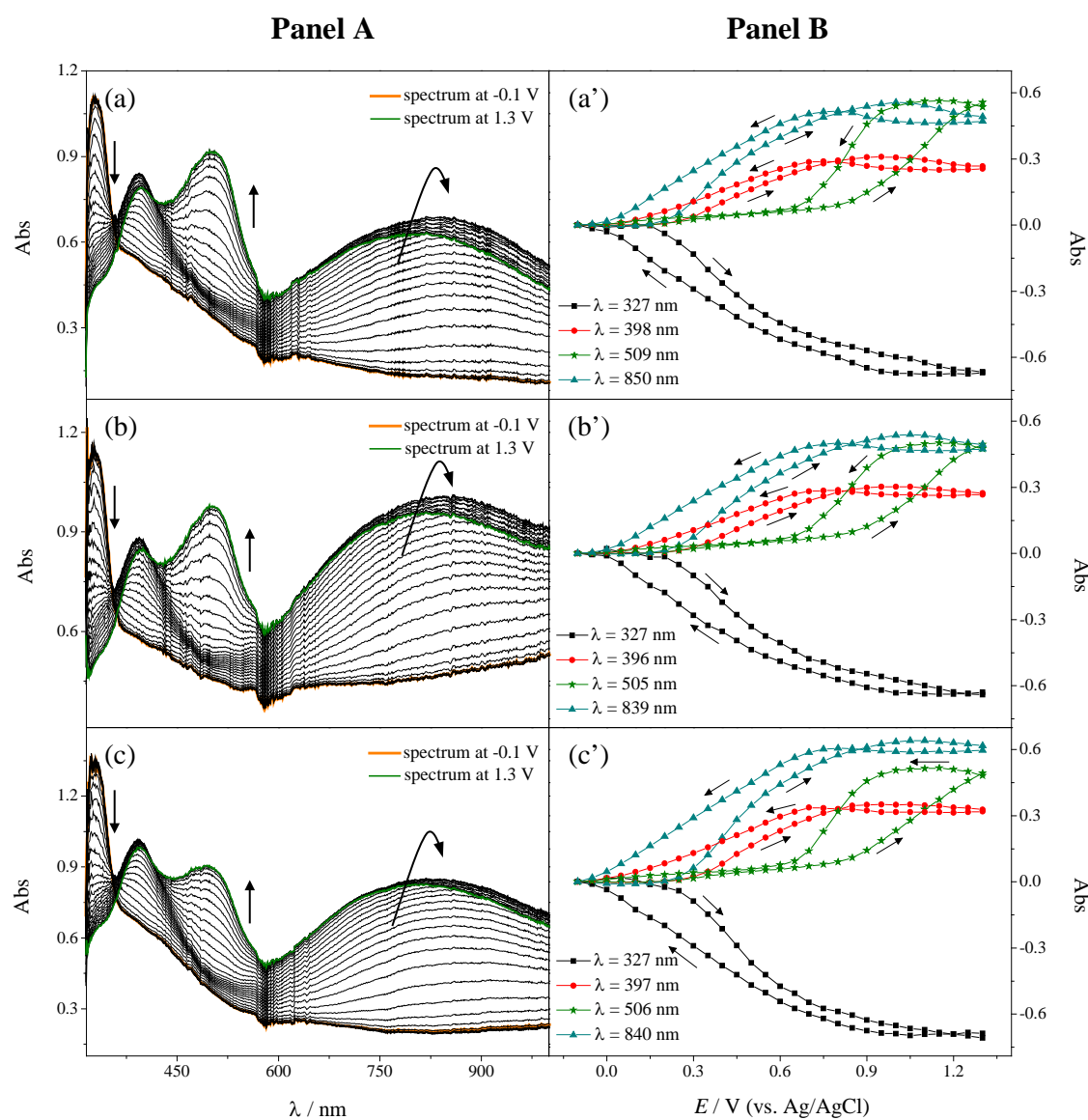


Figure 6. Panel A: Absolute UV-Vis spectra of (a) poly[1] ($\Gamma = 95.3 \text{ nmol cm}^{-2}$), (b) TiO₂@poly[1]_s and (c) TiO₂@poly[1]_r (prepared with 5 wt.% of TiO₂ NPs at $\nu = 0.020 \text{ V s}^{-1}$, $\Gamma = 104$ and 108 nmol cm^{-2} , respectively) acquired during film oxidation in $0.1 \text{ mol dm}^{-3} \text{ LiClO}_4/\text{PC}$ (referenced to the electrolyte spectrum). Panel B: *Abs* vs. *E* plots for the electronic bands identified in absolute UV-Vis spectra, referenced to spectra at $E = -0.1 \text{ V}$ (arrows indicate scan direction).

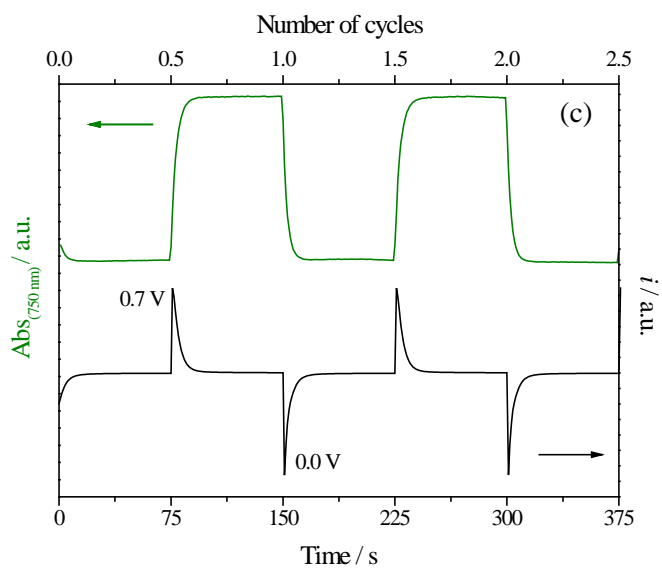
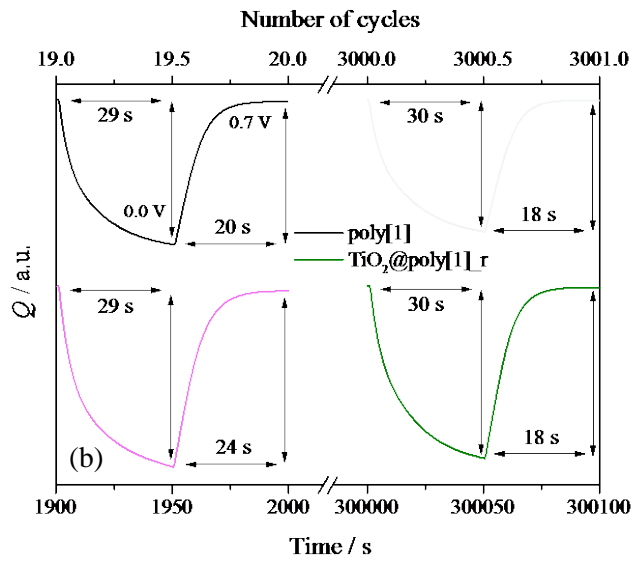
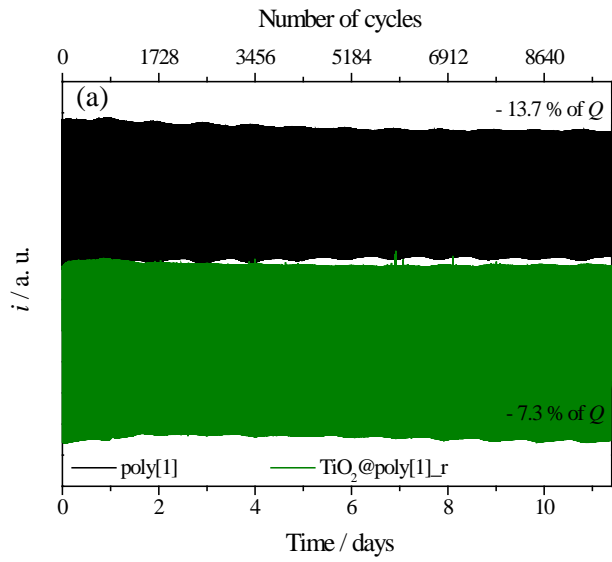


Figure 7. (a) Chronoamperograms of pristine and TiO₂@poly[1]_r films in LiClO₄/PC 0.1 mol dm⁻³, applying double potential steps (50 s duration each; 100 s for full redox cycle) between 0.0 V (yellow) and 0.7 V (green); (b) expansion of the chronoamperograms, showing the measured switching times at the 19th and 3000th cycles; (c) chronoamperograms/absorptograms obtained for TiO₂@poly[1]_r film, at the fixed wavelength of $\lambda = 750$ nm.

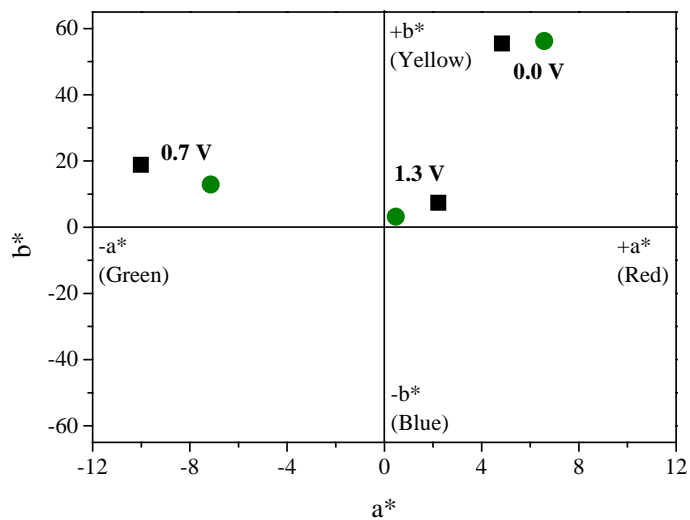


Figure 8. Graph of CIELAB colour values (a^* , b^*) of pristine (■) and nanocomposite $\text{TiO}_2@\text{poly}[1]_r$ (●) films, at different oxidation states: $E = 0.0$ V (yellow), $E = 0.7$ V (green) and $E = 1.3$ V (russet).

Tables

Table 1: XPS results: surface atom percentages and calculated atom ratios of selected elements for poly[1] pristine film and TiO₂@poly[1]_r nanocomposite, following emersion in their reduced states ($E = 0.0$ V).

| Sample | Atom % | | | | | Atom Ratios | | |
|--|--------|------|-----|------|-----|-------------|------|-------|
| | Ni | C | N | O | Cl | N/Ni | O/Ni | Cl/Ni |
| poly[1] | | | | | | | | |
| Before redox | 3.5 | 75.5 | 7.6 | 12.0 | 1.3 | 2.2 | 3.4 | 0.4 |
| After redox in CH ₃ CN | 2.5 | 64.8 | 6.4 | 22.4 | 3.9 | 2.6 | 9.0 | 1.6 |
| After redox in PC | 2.7 | 72.8 | 6.6 | 15.9 | 2.1 | 2.4 | 5.9 | 0.8 |
| TiO₂@poly[1]_r | | | | | | | | |
| Before redox | 3.3 | 76.4 | 7.6 | 11.5 | 1.2 | 2.3 | 3.5 | 0.4 |
| After redox in CH ₃ CN | 2.1 | 56.6 | 5.7 | 29.6 | 6.0 | 2.7 | 14.1 | 2.9 |
| After redox in PC | 2.9 | 74.3 | 6.6 | 14.6 | 1.6 | 2.3 | 5.0 | 0.6 |

Table 2: Wavelengths of the electronic bands and respective energies and molar extinction coefficients (ε) for poly[1] and TiO₂@poly[1] nanocomposites (prepared with 5 wt.% of TiO₂ NPs at 0.020 V s⁻¹).

| Film | λ / nm (eV) | $\varepsilon \times 10^{-3} / \text{mol}^{-1} \text{ dm}^3 \text{ cm}^{-1}$ |
|--|---------------------------------------|---|
| poly[1] | 327 (3.80) | 6.80 |
| | 398 (3.12) | 3.78 |
| | 509 (2.44) | 12.2 |
| | 850 (1.46) | 6.44 |
| TiO₂@poly[1]_s | 327 (3.80) | 6.81 |
| | 396 (3.14) | 3.57 |
| | 505 (2.46) | 11.8 |
| | 839 (1.48) | 6.12 |
| TiO₂@poly[1]_r | 327 (3.80) | 7.24 |
| | 397 (3.13) | 3.96 |
| | 506 (2.45) | 10.2 |
| | 840 (1.48) | 6.68 |

Table 3: EC parameters: optical contrast (ΔT %), change of the optical density (ΔOD), charge requirement (Q_d), and colouration efficiency (η) for pristine poly[1] and $TiO_2@poly[1]_r$ nanocomposite films in $LiClO_4/PC$ supporting electrolyte, at $\lambda = 750$ nm.

| Film | ΔT % | ΔOD | $Q_d /$ mC cm⁻² | $\eta /$ cm² C⁻¹ |
|-------------------------------------|--------------------------------|-------------------------------|---|---|
| poly[1] | 46.3 | 0.40 | 4.53 | 87.7 |
| $TiO_2@poly[1]_r$ | 43.4 | 0.48 | 5.45 | 87.5 |

Table 4: CIELAB colour values (L^* , a^* , b^*) and colour difference, ΔE^* , between different oxidation states of pristine and nanocomposite films.

| Film | E / V^a | L^* | a^* | b^* | E range / V | ΔL^* | Δa^* | Δb^* | ΔE^* |
|--|-----------------------------|-------------------------|-------------------------|-------------------------|---------------------------------|--------------------------------|--------------------------------|--------------------------------|--------------------------------|
| poly[1] | 0.0 | 63.2 | 4.8 | 55.4 | | | | | |
| | 0.7 | 31.9 | -10.0 | 18.8 | 0.0-0.7 | -31.3 | -14.8 | -36.6 | 50.4 |
| | 1.3 | 22.2 | 2.2 | 7.4 | 0.7-1.3 | -9.7 | 12.2 | -11.5 | 19.4 |
| TiO₂@poly[1]_r | 0.0 | 58.7 | 6.6 | 56.2 | | | | | |
| | 0.7 | 27.9 | -7.1 | 12.9 | 0.0-0.7 | -30.8 | -13.7 | -43.3 | 54.9 |
| | 1.3 | 20.6 | 0.5 | 3.2 | 0.7-1.3 | -7.3 | 7.6 | -9.7 | 14.3 |

^a Values at $E = 1.3$ V may be subject to uncertainty (see main text).

Table of Contents

